

# The 2001 $M_w$ 7.6 Bhuj earthquake, low fault friction, and the crustal support of plate driving forces in India

Alex Copley,<sup>1,2</sup> Jean-Philippe Avouac,<sup>1</sup> James Hollingsworth,<sup>1</sup> and Sébastien Leprince<sup>1</sup>

Received 1 December 2010; revised 19 May 2011; accepted 7 June 2011; published 19 August 2011.

[1] We present a source model for the 2001  $M_w$  7.6 Bhuj earthquake of northwest India. The slip distribution suggests a high stress drop ( $\sim 35$  MPa) and, together with the depth distribution of aftershocks, that the entire crust is seismogenic. We suggest that the active faults have an effective coefficient of friction of  $\sim 0.08$ , which is sufficient for the seismogenic crust to support the majority of the compressive force transmitted through the Indian lithosphere. This model is consistent with the midcrustal depth of the transition from extension to compression beneath the Ganges foreland basin where India underthrusts southern Tibet. If the coefficient of friction were the more traditional value of 0.6, the lithosphere would be required to support a net force roughly an order of magnitude higher than current estimates in order to match the observed depth of the neutral fiber.

**Citation:** Copley, A., J.-P. Avouac, J. Hollingsworth, and S. Leprince (2011), The 2001  $M_w$  7.6 Bhuj earthquake, low fault friction, and the crustal support of plate driving forces in India, *J. Geophys. Res.*, 116, B08405, doi:10.1029/2010JB008137.

## 1. Introduction

[2] The rheology of the continental lithosphere is a matter of ongoing debate. One view holds that long-term stresses are supported by the seismogenic crust [e.g., *Townend and Zoback, 2000; Jackson et al., 2008*], and another is that they are supported mainly by the lithospheric mantle [e.g., *Chen and Molnar, 1983; Watts and Burov, 2003; Hetényi et al., 2006*]. This debate has wide-ranging implications for our understanding of the past and present topography and deformation of continental regions.

[3] The  $M_w$  7.6 Bhuj earthquake, which struck northwest India on 26 January 2001, provides a rare chance to study a large intraplate earthquake and to probe the rheology of the Indian lithosphere. The earthquake was a reverse faulting event and occurred in a relatively stable part of the Indian subcontinent (Figure 1), where GPS measurements spanning the whole Indian peninsula indicate at most 2 mm/yr of internal shortening [*Bettinelli et al., 2006; Banerjee et al., 2008*]. Nonetheless, the Bhuj event and the  $M_w \sim 7.7$  Rann of Kachchh earthquake (which occurred  $\sim 100$  km to the west in 1819 [*Bilham, 1999*]), along with the faulting on the margins of the Shillong Plateau in northeast India [*Ambraseys and Bilham, 2003*], represent areas where the largely undeforming Indian lithosphere is breaking. The deformation is probably a response to the force associated with the India-Asia collision. Given that it is possible to estimate the magnitude of this force [e.g., *Molnar and Lyon-Caen, 1988; Copley et al., 2010*], the Bhuj earthquake offers

an opportunity to study a large event in a region where the magnitude of the total force transmitted through the lithosphere is known, thereby allowing the rheology to be investigated. The aim of this paper is to describe a new source model for the event, obtained from the joint inversion of seismic and geodetic data sets, and to use the results to probe the rheology of the Indian lithosphere.

## 2. Slip Model

### 2.1. Data and Method

[4] The Bhuj earthquake has been studied previously using seismic and geodetic methods [*Antolik and Dreger, 2003; Chandrasekhar et al., 2004; Schmidt and Bürgmann, 2006*], and this paper builds upon these studies by combining the existing data sets in a joint inversion for the spatial and temporal distribution of slip on the fault plane while incorporating newly acquired surface offset data derived from SPOT satellite imagery. We simultaneously invert 21  $P$  and 19  $SH$  teleseismically recorded waveforms along with surface displacements measured using interferometric synthetic aperture radar (InSAR) [*Schmidt and Bürgmann, 2006*] and the reoccupation of leveling lines [*Chandrasekhar et al., 2004*]. We constrain the moment to be the same as the centroid moment tensor (CMT) solution ( $3.4 \times 10^{20}$  N m) and find the best fitting distribution of slip, rake, rupture velocity, and rise time on planes divided into 5 km wide square patches. The inversions are performed using a simulated annealing algorithm to find the model that best fits the geodetic data and the wavelet transform of the seismograms (for a more complete description of the method used, see *Ji et al. [2002]* and *Konca et al. [2008, 2010]*). We weight the seismic and geodetic data such that they have equal importance in the inversions, in the sense that the contribution of the weighted residuals of each type of data to the total misfit is equal. This approach is supported by the observation that the increase in residuals for

<sup>1</sup>Tectonics Observatory, Division of Geological and Planetary Sciences, California Institute of Technology, Pasadena, California, USA.

<sup>2</sup>Now at COMET+, Bullard Laboratories, Department of Earth Sciences, University of Cambridge, Cambridge, UK.

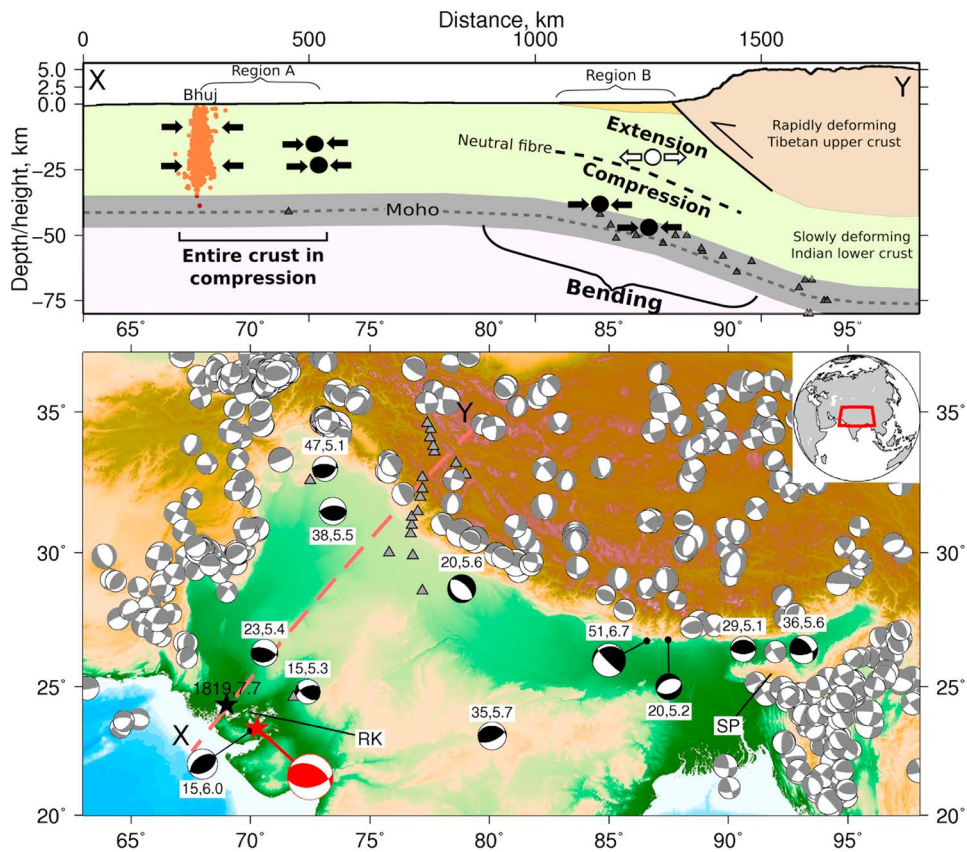


**Figure 1.** (bottom) Seismicity of northern India and surroundings. Gray focal mechanisms are from the CMT catalog. Those shown in black are within Indian lithospheric material and are labeled with the centroid depth in km and the moment magnitude; focal parameters are listed in Table S1. Our focal mechanism for the Bhuj earthquake is shown in red. SP, Shillong Plateau; RK, Rann of Kachchh. (top) Cross section showing the aftershocks of the Bhuj earthquake (red circles, [Bodin and Horton, 2004]) and the locations of earthquakes shown on the map within 400 km of the line of section (black circles, reverse faulting; white circles, normal faulting). Also shown are receiver function estimates of Moho depths (gray triangles [Priestley et al., 2008]).

each of the data sets when used in the joint inversion, compared to when used individually, is small and equal ( $<4\%$ ). We assume that the preseismic and postseismic contribution to the geodetic data is minor and that we can therefore use the data to invert for the coseismic slip distribution. The very low rates of deformation within peninsular India [Bettinelli et al., 2006; Banerjee et al., 2008] suggest that the preseismic deformation is indeed minor. Chandrasekhar et al. [2009] measured geodetic displacements from 3 months to 6 years after the event and found displacements of  $\leq 2$  cm, which is minor compared with the meter-scale deformation observed in the geodetic data spanning the main shock. Given the extensive reports of liquefaction features [Wesnousky et al., 2001], a possible source of postseismic ground deformation is the shallow movement of groundwater. However, we suggest that this forms only a minor component of the geodetic observations because the data show a smoothly varying displacement field that is unaffected by variations in surface geology (e.g., basins and bedrock ranges). Additionally, the InSAR data only cover regions where liquefaction was minor or absent, otherwise the ground disruption would cause a loss of coherence. We

therefore assume that the observed geodetic deformation is dominated by the coseismic signal.

[5] We use a fault plane with a strike of  $82^\circ$  and a southward dip of  $51^\circ$ , as determined from teleseismic body wave modeling [Antolik and Dreger, 2003]. When combined with the hypocentral location in the Engdahl, van der Hilst, and Buland (EHB) catalog, this plane lies along a planar zone of aftershocks [Bodin and Horton, 2004] and is consistent with post-earthquake coastline changes in the Rann of Kachchh lagoon [Gahalaut and Bürgmann, 2004]. We use a fault that is larger in size (65 km along-strike and 40 km downdip) than our resulting slip distribution so that our results are not constrained by the fault extent.

[6] Optical satellite images can be analyzed with the COSI-Corr software [Leprince et al., 2007, 2008] in order to observe subpixel-sized surface deformation. This technique yields displacement maps for the components of motion in the N-S and E-W directions and is sensitive to displacement discontinuities rather than absolute values of displacement and long-wavelength signals. If the satellite look angle is not vertical (as is the case with the available images spanning the time of the Bhuj earthquake), then a component of

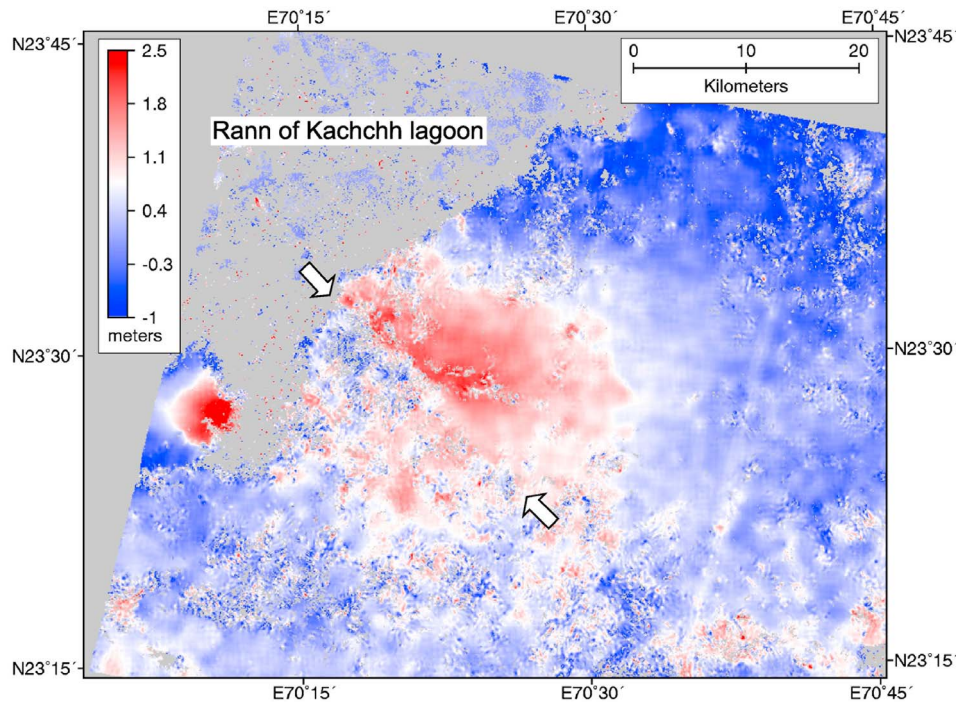


**Figure 2.** The E-W and vertical components of the surface displacements measured from SPOT images (i.e., eastward displacements plus the vertical uplift multiplied by  $\tan(22.7^\circ)$ ; see text and Figure S1). The method is sensitive to displacement discontinuities rather than to absolute values of displacement and long-wavelength signals. The robust feature in the image is the discontinuity marked by white arrows, corresponding to a displacement discontinuity of  $\sim 0.6$  m averaged along the rupture.

any vertical motion that occurs will appear in the east-west displacement map as an apparent horizontal displacement. The image geometry is shown in Figure S1 along with a detailed explanation of how both horizontal and vertical motions contribute to the observed signal.<sup>1</sup> We have applied this technique to the Bhuj earthquake and have observed a  $\sim 15$  km long NW-SE trending displacement discontinuity (Figure 2). This feature represents a secondary fault, in addition to that described above, which accumulated surface displacement and which we also include in our inversion. The strike of the secondary fault is inconsistent with the seismically derived focal mechanisms for the Bhuj earthquake, indicating that moment release on this fault was minor compared with that on the main plane. Because of the oblique incidence angle of the satellite images, the observed signal in the east-west displacement map shown in Figure 2 corresponds to the east-west displacement (with eastward being positive) plus the vertical uplift multiplied by  $\tan(22.7^\circ) = 0.42$  (the satellite was looking to the east with an incidence angle of  $22.7^\circ$ ). We see a signal of  $\sim 0.6$  m (averaged along the secondary fault) in this E-W and vertical component and no discernible offsets in the N-S component (which limits the deformation to be less than  $\sim 0.4$  m; see Figure S2). The fault we have imaged corresponds to the location of the surface faulting documented in the field by *Wesnousky et al.* [2001]. However, the displacement we measure is larger than that reported in the field (which was up to 36 cm right-lateral strike slip) and

extends for a greater distance along-strike ( $\sim 20$  km compared with 8 km). This discrepancy may be due to the field measurements being complicated by large zones of diffuse deformation [*Wesnousky et al.*, 2001]. A similar effect was seen in the 1999  $M_w$  7.1 Duzce (Turkey) earthquake, where the surface offsets measured from optical image correlations form an upper envelope to the field measurements of the slip on the fault scarp. Such a pattern suggests that some of the slip was not localized onto the surface rupture but was diffuse deformation in the immediate vicinity [*Konca et al.*, 2010]. In summary, for the surface rupture on this secondary fault plane, our results indicate  $< 0.4$  m N-S displacement and  $\sim 0.6$  m of eastward displacement plus the uplift component. When combined with the condition that the amount of right-lateral strike slip must be at least 36 cm [*Wesnousky et al.*, 2001], a grid search of parameters reveals that these results constrain the fault plane to be steeply dipping ( $\geq 80^\circ$  to the NE) with 0.6–1.5 m of slip and a rake of  $100$ – $160^\circ$ . In our inversions we impose these conditions on the surface slip of the secondary fault plane.

## 2.2. Inversion Results

[7] Figure 3 shows the results of our inversion. There is a well-known trade-off between the quality of the fit to the data and the smoothing imposed upon the model [e.g., *Jónsson et al.*, 2002]. Our preferred model, shown in Figure 3, is the smoothest solution which does not significantly degrade the fit to the data. The model yields good fits to all the data sets. Figure 4 shows the observed and modeled teleseismic P and SH waveforms. Figure 5

<sup>1</sup>Auxiliary material files are available in the HTML. doi:10.1029/2010JB008317.

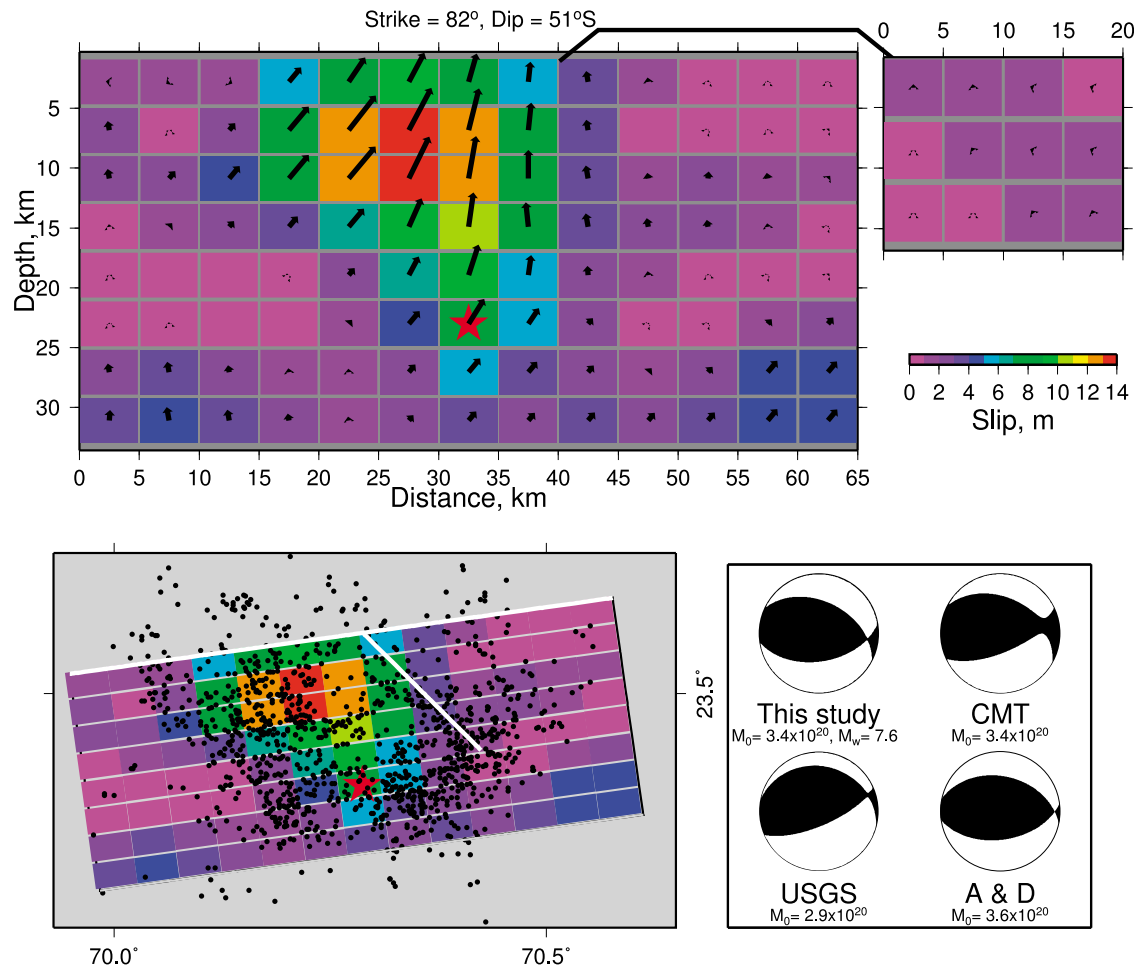


**Figure 3.** (top) Our calculated slip distribution for the Bhuj earthquake. The red star shows the hypocenter, and the black line shows where the two planes intersect at the surface. (bottom) (left) Map view of the surface intersections of the two fault planes (white lines) and the locations of aftershocks recorded by *Bodin and Horton* [2004]. (right) A comparison of focal mechanisms for the earthquake. A & D, *Antolik and Dreger* [2003].

shows the fit between the observed and modeled surface deformation. The leveling data [*Chandrasekhar et al.*, 2004] are everywhere fit to within the error on the measurements, and the RMS misfit to the InSAR data [*Schmidt and Bürgmann*, 2006] is 6.5 cm, which is of a similar magnitude to commonly observed atmospheric effects. *Schmidt and Bürgmann* [2006] were only able to measure ground displacements using InSAR within isolated patches, which mostly did not extend far enough from the fault for the earthquake-related displacement to decay to zero. We therefore only fit the relative line-of-sight displacements within each patch during the inversions. Some of the InSAR patches in Figure 5 show spatially organized misfits between the data and model predictions. These are likely to be atmospheric in origin because descending-track data patches from different SAR image pairings, but similar image geometries, show opposite senses in the gradients of data-model misfit for the same regions (i.e., Figures 5e and 5f suggest that our computed E-W ground displacement gradient is too low, whereas Figure 5c suggests that it is too high). This suggests that errors in our estimated ground displacements cannot be the cause of the misfits because if this were the case the

data from the same image geometries would show the same gradients of data-model misfit. Support for an atmospheric origin for these signals comes from the observations of *Schmidt and Bürgmann* [2006], who noted large atmospheric signals in the InSAR results from the region, and from the postseismic InSAR data of *Chandrasekhar et al.* [2009], who showed atmospheric effects of a similar magnitude to our inversion residuals. The minor slip in the bottom corners of the fault plane, away from the high-slip patch, represents inversion artifacts.

[8] As can be seen from Figure 5, the InSAR and leveling data tightly constrain the lateral extent of the surface deformation and hence the coseismic rupture. The mean rupture velocity within the region of high slip is estimated to be  $\sim 2.2\text{--}2.4$  km/s, similar to other large thrust-faulting earthquakes [e.g., *Ji et al.*, 2003; *Avouac et al.*, 2006]. The surface strain that we compute from our model agrees with the observations of *Wallace et al.* [2006], which were not used in the inversions because of reference frame uncertainties (see Figure S4).

[9] Our model shows a remarkably compact source, with slip of up to 14 m occurring in a ruptured patch which is

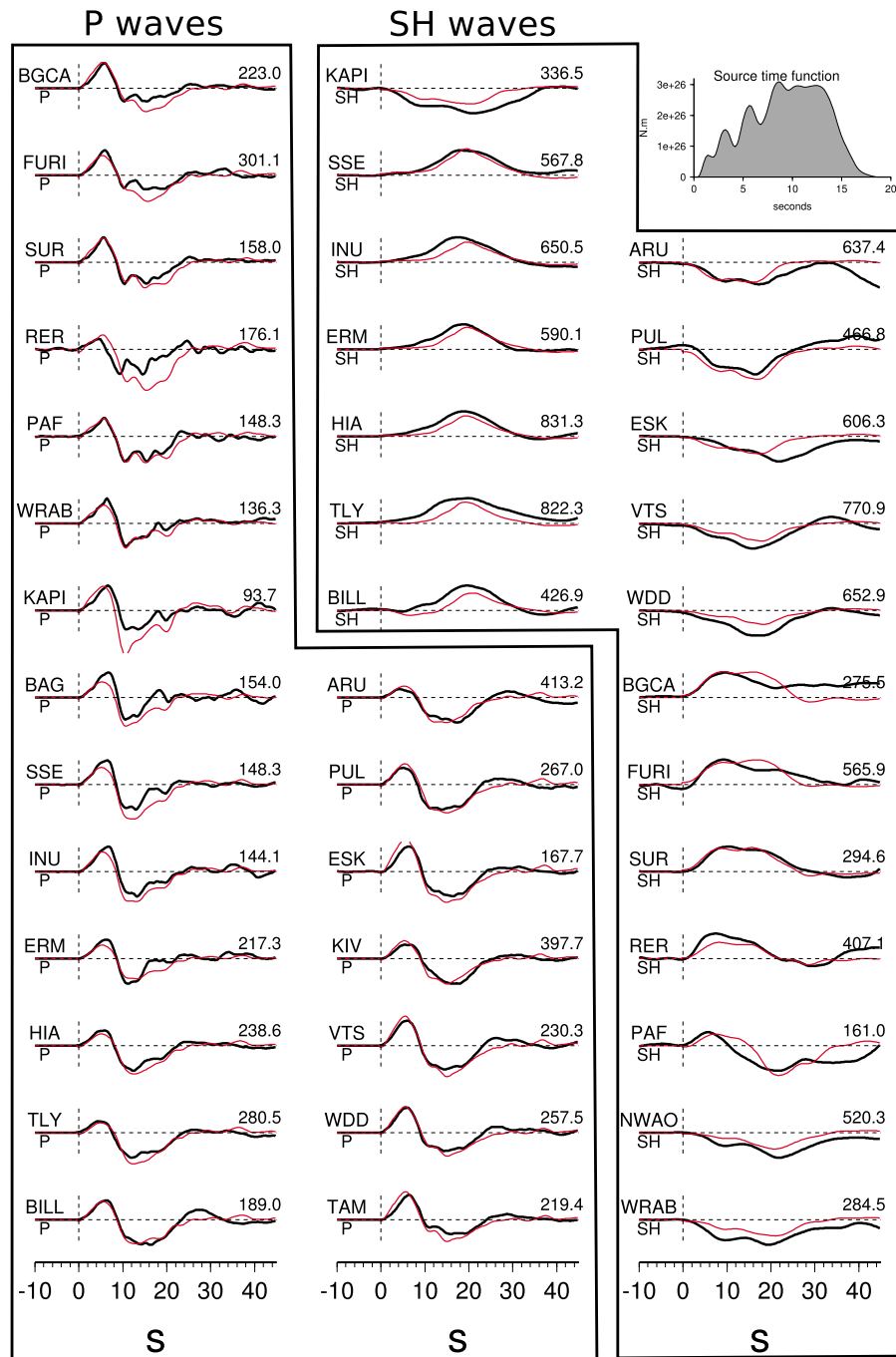


**Figure 4.** Observed (black) and modeled (red) teleseismic waveforms. The maximum amplitude of each seismogram is shown on the right of the trace. The inset at top right shows the source time function of our model. The station distribution is shown in Figure S3.

~30 km wide. The slip model shows broad slip maxima flanked by large slip gradients on the margins. This is the same form as is predicated by the analytic solutions of *Bürgmann et al.* [1994] for slip on a circular crack, in which the slip distribution depends upon the size of the slipped patch and the stress drop during the event. We can therefore estimate the stress drop by fitting the expressions of *Bürgmann et al.* [1994] to the along-strike variation of displacements through the slipped region in our source inversions. This estimate is 35 MPa. Figure 3 shows that

the majority of the aftershocks recorded 2.5–5.5 weeks after the mainshock [*Bodin and Horton, 2004*] are concentrated at the edges of the slipped patch, suggesting they are related to stress concentrations on the margins of the coseismic rupture. The similarity of the *P* axes of the aftershocks and the main shock [*Bodin and Horton, 2004*] probably indicates that the postseismic deformation is primarily due to continued motion on the lateral edges of the coseismic slip patch, with a similar rake to the main event. The secondary fault only slipped at shallow depths and intersected the main

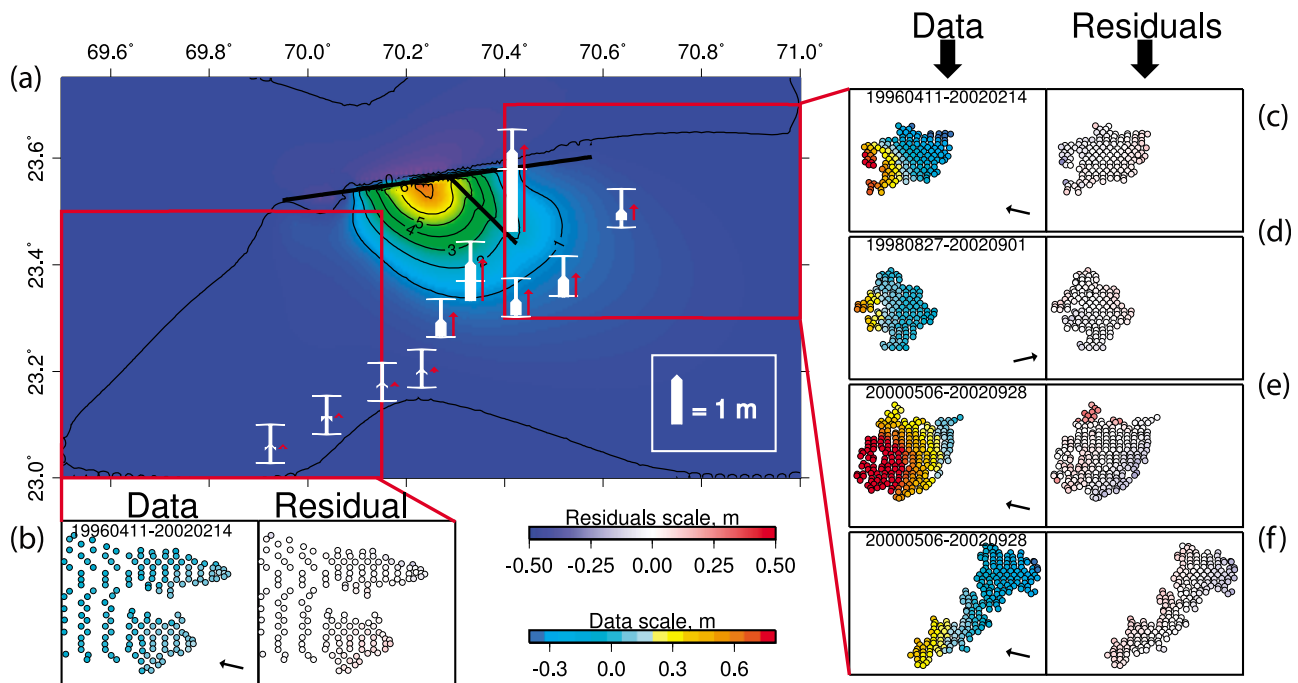


**Figure 5.** Fits between the modeled and observed surface deformation. (a) The modeled line-of-sight displacement for a descending-track SAR interferogram with the contours labeled in meters. The thick black lines show the surface intersections of the main and secondary model fault planes. The white bars with error bounds show vertical displacements measured by *Chandrasekhar et al.* [2004], and the red arrows show the model predictions at the same locations. (b–f) The InSAR results of *Schmidt and Bürgmann* [2006] labeled with the dates of the SAR images used, along with the residuals between the data and the model (shown as the data value minus the model prediction). The small black arrows show the satellite look direction. Figures 5c–5f all cover the geographical area, as shown by the easternmost red box in Figure 5a.

fault plane in a region of large along-strike slip gradients, suggesting that it ruptured the shallow crust in response to the stresses resulting from the large displacement gradients on the main fault plane.

[10] The details of the slip distribution shown in Figure 3 depend upon the moment we have used (taken from the CMT solution) and the degree of smoothness we have imposed upon the inversion. The results of inversions using different seismic moments are shown in Figures S5 and S6 (with the moment varying from 10% higher to 20% lower than the CMT solution in order to encompass the estimates of *Antolik and Dreger* [2003] and the U.S. Geological Survey, which were 6% higher and 15% lower, respectively). We have also shown the results of an under-smooth calculation (Figure S7) where there are large and physically unrealistic variations in slip and rake over short distances within the high-slip region (the solution shown is twice as rough as that shown in Figure 3). Over-smooth calculations are not able to fit the geodetic data adequately because the displacement field spreads over a wider area than is seen in the InSAR data, and the results of such a calculation are shown in Figure S8 (where the solution is half as rough as that shown in Figure 3). However, the broad features of all these solutions are the same as shown in Figure 3. All the models require that there is a compact source with high slip, and these additional calculations can be used to place error

estimates on the parameters of interest. Specifically, we estimate an error bound of 10 MPa for our calculated stress drop in order to encompass all of the values derived from the “extreme parameter” inversions described above (these results are summarized in Table S2). We conclude that the seismological and geodetic data available for this earthquake require a deep source (extending below 20 km) and a large stress drop ( $35 \pm 10$  MPa). These are robust conclusions in view of the uncertainty in the data and the modeling parameters. Finally, we note that if a significant postseismic signal contributed to the geodetic data we used for the source inversion, we would overestimate the size of the slipped patch (because this deformation would relax the stress concentrations at the tip of the rupture). We would therefore underestimate the stress drop. However, because the observed postseismic signal was minor [*Chandrasekhar et al.*, 2009], if this underestimate is present, then the true value is likely to be well within our estimated error bounds.

[11] We have performed a series of calculations with alternative fault geometries (by varying the strike, dip, and location of the fault). These calculations all show increased misfits between the data and the model predictions, indicating that we have selected the correct fault geometry for our inversions. The inversions with the smallest increases in misfit are those with geometries closest to the one used for the calculation shown in Figure 3, and in these cases the slip

distributions and calculated stress drops are very similar to those shown in Figure 3 (as illustrated in Figure S9).

### 2.3. Comparison With Previous Studies

[12] Figure 3 shows the focal mechanism calculated from our slip model to be consistent with those of previous studies (including the CMT solution). According to our model, the main surface rupture lies within the Rann of Kachchh lagoon. No primary surface faulting was observed during fieldwork studies following the earthquake. However, shallow deformation within the lagoon is consistent with the changing patterns of seasonal flooding described by *Gahalaut and Bürgmann* [2004]. Given the lack of surface rupture, it is possible that the shallow deformation may have been distributed within the thick sediments of the lagoon, rather than localized onto a single discrete surface. Alternatively, the slip may have died out as the rupture propagated close to the surface (as suggested by *Johanson and Bürgmann* [2010] for the San Simeon earthquake). Unfortunately, our data set does not provide good enough resolution to resolve the very shallow slip and to distinguish between these possibilities. The distributed slip model of *Antolik and Dreger* [2003] has less slip at the surface than does our model, although the deepest extent of faulting is similar. However, in their slip model *Antolik and Dreger* [2003] found an anomalously low moment (only 60% of their point source solution), and we suggest that the discrepancy in surface slip between the models results from the deficit of moment in the *Antolik and Dreger* [2003] solution. By inverting InSAR data, *Schmidt and Bürgmann* [2006] suggested that the updip edge of the fault plane was at a depth of 9–15 km. However, we are able to fit the same InSAR data with a model in which slip reaches the surface. In order to test which of these alternatives provides a better fit to the full range of seismic and geodetic data sets, we have performed inversions in which we constrain the upper 10 km of our fault plane to have zero slip (although we allow surface slip on the secondary fault plane, which the SPOT image correlation shows must have accumulated shallow slip). In this case we find that the misfit to the data increased by ~10% and the solution has a physically unlikely slip discontinuity (with the displacement reducing from ~9 m to zero between the cells centered on a downdip distance of 12.5 km and those centered at 7.5 km; see Figure S10). We therefore prefer our model in which slip reaches the surface. The differences between our model and that of *Schmidt and Bürgmann* [2006] are likely to be mainly due to the additional data sets we use and also to a lesser extent to our use of a variable-slip model rather than one in which a rectangular fault plane has a constant slip. Note that models with less slip near the surface (see Figure S10) have a more compact source and therefore higher stress drop than our preferred model shown in Figure 3.

[13] Our calculated stress drop is greater than that estimated by *Negishi et al.* [2002] and *Bodin and Horton* [2004], and the difference is due to the methods used. We estimated the stress drop directly from our slip model. *Negishi et al.* [2002] and *Bodin and Horton* [2004] used the locations of aftershocks to estimate the size of the fault plane and then used the moment of the earthquake to estimate the stress drop. Figure 3 shows that many aftershocks actually concentrated beyond the edges of the slip patch, resulting in these previous

studies slightly overestimating the size of the slipped patch and so underestimating the stress drop.

## 3. Implications for the Rheology of the Indian Lithosphere

### 3.1. Minimum Estimate of Coefficient of Friction

[14] Our estimate of the stress drop ( $35 \pm 10$  MPa) provides a lower bound on the pre-earthquake shear stress on the fault plane, averaged over the rupture (which had a centroid depth of 14 km). The bound is a lower one because it is possible that not all of the shear stress on the fault plane was released by the earthquake. For comparison, *Seeber et al.* [1996] estimated a stress drop and centroid depth for the  $M_w$  6.1 1993 Killari earthquake in southern India of 4.5–10 MPa and 2.6 km. The pattern of increasing stress drop with depth implied by these earthquakes suggests that we can discuss the rheology of the region by estimating a single coefficient of friction ( $\mu$ ) for the seismogenic crust, defined as the ratio of the shear and normal stress on the fault at failure. The normal and shear stresses are given by  $\sigma_n = \rho gz + (\Delta\sigma_{xx}/2)(1 + \cos 2\theta)$  and  $\tau = -(\Delta\sigma_{xx}/2) \sin 2\theta$  where  $\rho$  is the density,  $\Delta\sigma_{xx}$  is the horizontal deviatoric stress, and  $\theta$  is the angle between the fault and the vertical [e.g., *Turcotte and Schubert*, 2002]. Our minimum estimate of  $\tau$  can therefore let us estimate  $\Delta\sigma_{xx}$ , which in turn allows us to use the centroid depth to calculate  $\sigma_n$ . The ratio of  $\tau$  and  $\sigma_n$  then allows us to estimate that  $\mu \geq 0.08 \pm 0.02$  (a lower bound on the shear stress gives rise to a lower bound on  $\mu$ ). Following the same method, *Seeber et al.*'s [1996] estimate of the stress drop and centroid depth of the 1993 Killari earthquake yields a similar estimate of  $0.09 \pm 0.03$ . Given the agreement of these estimates from different centroid depths, we assume that the coefficient of friction we have estimated applies to the entire seismogenic depth range within the Indian crust. This low estimate of the coefficient of friction is compatible with the relatively steep dips of the Bhuj and Killari fault planes, along with other events shown on Figure 1 and the faulting on the margins of the Shillong Plateau [*Bilham and England*, 2001].

### 3.2. Maximum Estimate of Coefficient of Friction

[15] Here we estimate the maximum possible coefficient of friction that allows brittle failure to occur in response to the plate driving forces transmitted through the Indian lithosphere. The pervasive seismicity located throughout the Indian shield revealed by historical records [e.g., *Rao and Rao*, 1984; *Rao*, 2000], as well as evidence for significant and sustained deformation of the Indian crust in the Shillong Plateau region in particular, support the assumption that the condition for failure has also been reached in regions other than Bhuj. The distribution of coseismic slip and the aftershocks of the Bhuj earthquake [*Mandal et al.*, 2006] show the entire 44 km thickness of the crust in the area [*Mishra et al.*, 2005; *Sarkar et al.*, 2007] to deform by brittle failure. It is possible that the deep aftershocks could represent a temporary deepening of the brittle-ductile transition due to the postseismic increase in strain rate, and the depth extent of coseismic slip could reflect dynamic propagation of the rupture below that transition. However, the deepening of the brittle-ductile transition following earthquakes is generally found to be small, if detectable at all [e.g., *Rolandone et al.*, 2004].

[16] The depth extent of brittle faulting across the Indian peninsular mirrors that seen at Bhuj. For example, Figure 1 shows that seismicity  $\sim 1000$  km to the east of the Bhuj earthquake has occurred to depths of at least 35 km, and *Priestley et al.* [2008] discussed seismicity throughout the entire thickness of the crust in northeast India and where India underthrusts Tibet. The spatially distributed teleseismically recorded and microseismic deformation of the Indian lithosphere, in response to both tectonic and reservoir-induced stresses (e.g., the Koyna reservoir [*Gupta, 2002*]), shows that large areas of the subcontinent are on the verge of failure. The focal mechanisms of the earthquakes (thrust faults with  $P$  axes directed toward the Tibetan Plateau), and the thrust faulting on the margins of the Shillong Plateau [*Bilham and England, 2001*], suggest that this deformation represents the Indian plate breaking in response to the force exerted upon it by the Tibetan Plateau.

[17] By studying the slowdown of India at the time of onset of the India-Asia collision, *Copley et al.* [2010] estimated the magnitude of the force exerted upon India by the Tibetan Plateau to be  $\sim 5.5 \pm 1.5 \times 10^{12}$  N/m along-strike (similar to *Molnar and Lyon-Caen's* [1988] estimate of  $\sim 6.9 \times 10^{12}$  N/m, from considering crustal thickness contrasts). By assuming that the crust supports the entirety of the force transmitted through the lithosphere, we can therefore estimate an upper limit for  $\mu$  in the crust, which is  $0.09 \pm 0.02$  for surfaces with the same dip as the fault plane ruptured by the Bhuj earthquake. If  $\mu$  were any higher, the forces imposed upon the Indian plate would be too small to cause active faulting.

[18] Our estimated maximum value of  $\mu$  represents an upper limit on the vertical integral of the stress distribution. It is possible that the stress could be highly heterogeneous with depth, and the observed earthquakes could represent areas which are locally reaching failure with a higher value of  $\mu$ . However, topographic features built by active faulting in regions such as the Shillong Plateau and the Rann of Kachchh lagoon suggest that repeated earthquakes must have occurred. In order to allow elastic strain to repeatedly accumulate, deformation must occur throughout the entire thickness of the seismogenic layer. Because of this we believe that the earthquakes cannot represent stress heterogeneities with depth within a largely undeforming crust, and that our estimate of  $\mu$  does represent an upper bound for the stress which is supported by the Indian crust.

### 3.3. Low-Friction Faults Extending Into a High-Viscosity Lower Crust

[19] The minimum and maximum values of  $\mu$  we have estimated are in close agreement, suggesting three conclusions. First, the stress level within the Indian crust is limited by faults with a coefficient of friction similarly low to that seen at Bhuj, otherwise there would be no earthquakes within peninsular India. Second, although the faults have a low coefficient of friction, they are able to support the majority of the force transmitted through the Indian plate. This conclusion is consistent with the findings of *Chandrasekhar et al.* [2009], who used postseismic deformation following the Bhuj earthquake to suggest that the lithospheric mantle in the region was weak (with a viscosity of  $2 \times 10^{19}$  Pa s). Finally, the Bhuj earthquake must have relieved most or all of the shear stress on the fault plane,

otherwise the fault would have been able to support enough stress that it would not have ruptured in response to the applied forces.

[20] Our estimate of  $\mu$  on the Bhuj fault plane corresponds to the faults supporting a total horizontal force of  $4.9 \pm 1.2 \times 10^{12}$  N/m. The solid line in Figure 6a shows the distribution of differential stress in the crust computed from our estimate of  $\mu$ . By using this distribution of stress, we can calculate that the effective viscosity of the lower crust must be  $\geq 10^{24}$  Pa s in order to prevent ductile flow occurring at the strain rate estimated by *Bettinelli et al.* [2006] (equivalent to 2 mm/yr distributed over a horizontal distance of 1000 km). Such ductile behavior would be inconsistent with the observations of seismicity extending as deep as the Moho. This lower limit on the effective viscosity is similar to that of *Copley et al.* [2011], who used the spatial pattern of strain within the Tibetan Plateau to obtain a lower bound of  $5 \times 10^{23}$  Pa s for where India underlies southern Tibet.

[21] The thick dashed line in Figure 6a shows an upper limit on the stresses in the mantle under the assumption that these stresses accommodate the remaining  $0.6 \times 10^{12}$  N/m of *Copley et al.'s* [2010] estimated total compressive force. This curve was calculated by using the olivine diffusion creep activation energy of *Hirth and Kohlstedt* [2003] and the geotherm of *Priestley et al.* [2008] (recalculated for the larger crustal thickness in the Bhuj region than was originally used) to give the variation of stress with depth. We then adjusted the other flow law parameters to obtain the required vertically integrated stress. The curve is an upper limit on the stress distribution, as some of the force could be supported along-strike of the fault or as unrelieved stresses on the Bhuj fault plane.

[22] A coefficient of friction as low as 0.08 requires the presence of minerals with intrinsically low friction (e.g., certain clay minerals or a powdered gouge of the surrounding rock) or of fluids at  $\sim 85\%$  of the lithostatic pressure (assuming a “dry”  $\mu$  of 0.6). Borehole observations that fluid pressures in the continental crust are close to hydrostatic [e.g., *Townend and Zoback, 2000*] may appear to rule out elevated fluid pressures. However, *Sleep and Blanpied* [1992] discussed the potential for high pore pressures to be localized along active fault planes. Also, it is possible that the length scale for pore fluid pressure perturbations [e.g., *McKenzie, 1984*] (which could be induced, for example, by drilling) may be similar to, or larger than, the length scales observed by individual measurements in the borehole experiments [e.g., *Huenges et al., 1997*]. We therefore do not believe that we can distinguish between the possible causes for the low value of  $\mu$ . However, our estimate of 0.08 is compatible with *Bollinger et al.'s* [2004] conclusion, based on topographically induced stresses, that  $\mu$  is less than 0.3 on the Main Himalayan Thrust and with *Herman et al.'s* [2010] estimate of an upper bound for  $\mu$  of 0.07 for the same fault. Additionally, *Suppe* [2007] concluded that the topography in Taiwan is supported by faults with  $\mu$  of 0.04–0.1, and *Lamb* [2006] estimated 0.032–0.095 for  $\mu$  on subduction megathrusts. Therefore, in this respect, the Bhuj fault may not be atypical, and friction on faults in relatively stable areas may be as low as in rapidly deforming regions.

[23] In the above discussion, we assumed that the Bhuj region was representative of the rheology of the entirety of

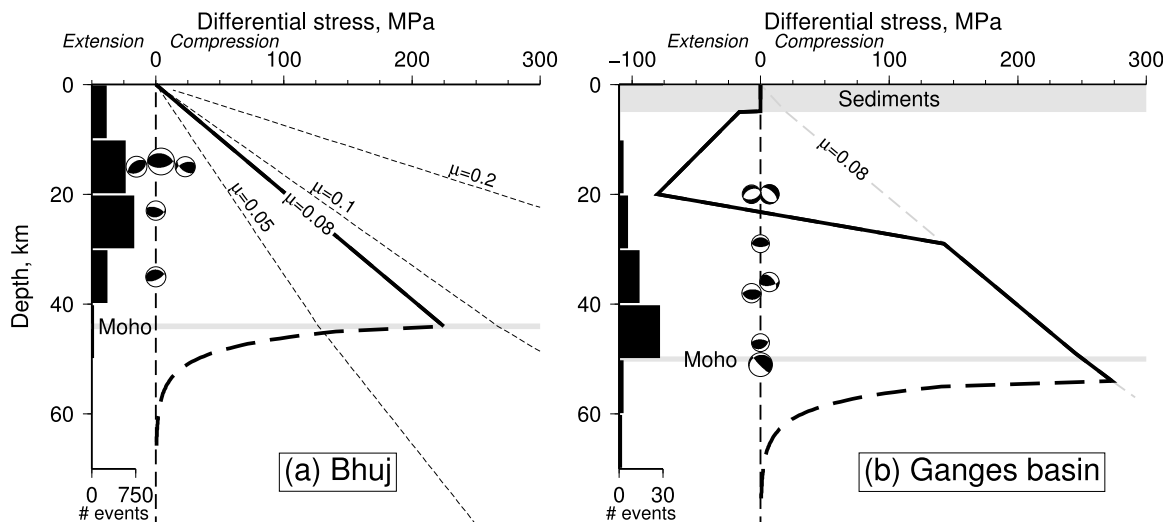


**Figure 6.** The thick lines show the distribution of differential stress with depth (solid, brittle regime; dashed, ductile regime) at Bhuj and beneath the Ganges foreland basin (regions A and B on Figure 1). The histograms on the left of each graph show the depth distribution of aftershocks following the Bhuj earthquake (Figure 6a, from *Mandal et al.* [2006]) and of earthquakes in eastern Nepal, south of the Main Central Thrust (Figure 6b, from *Monsalve et al.* [2006]). The lower hemisphere focal mechanisms of earthquakes shown in black on Figure 1 are shown in Figure 6b for events within 500 km of the Himalaya and otherwise in Figure 6a.

peninsular India. This view is strengthened by the agreement in estimates of  $\mu$  calculated from the Bhuj and Killari earthquakes, which occurred  $\sim 1000$  km apart. It should be emphasized that we do not think it likely that the entirety of the Indian subcontinent is permeated with weak faults, and some relatively strong and unfaulted regions presumably do exist. However, the Indian crust has experienced plentiful recent and historically recorded seismicity [e.g., *Rao and Rao*, 1984; *Rao*, 2000], much of it extending to lower crustal depths (Figure 1 and *Bilham and England* [2001]). This seismicity may possibly represent regions of reactivated ancient faulting [e.g., *Rao et al.*, 2002] (including the Bhuj region, which occurred in the region of a failed Mesozoic rift [*Talwani and Gangopadhyay*, 2001]). Regardless of if this is the case, the widespread earthquakes indicate that there are large areas in which faulting extends into the lower crust. It is these seismically active areas that we assume are plentiful enough that they limit the stress that can be transmitted through the Indian subcontinent as a whole, and we take the rheology in these regions to be the same as at Bhuj.

[24] There is some possibility that the local stress distribution in the Bhuj region may not be representative of the stress within the whole Indian subcontinent, for example because of the flexural effects related to Himalayan tectonics or the buckling of the Indian lithosphere. However, it is the rheology that we are taking as representative of the Indian peninsular, not the local configuration of forces.

#### 4. Consistency With Ganges Foreland Basin Seismicity

[25] Where India underthrusts the Himalaya, normal and reverse faulting earthquakes show that the upper crust is in extension and the lower crust and upper mantle are in compression (Figure 1), which places further constraints

upon the rheology of the Indian lithosphere. The variation of stress regime with depth must reflect the stresses induced by bending the Indian lithosphere at the front of the Himalaya, in addition to the net compression transmitted through the lithosphere. The transition from extension to compression occurs at a midcrustal depth of  $25 \pm 5$  km and suggests a single elastic core with the lithosphere failing in extension above it and compression below it. The presence of only one elastic core is qualitatively consistent with the rheological model we proposed for peninsular India. We can use our rheological model to calculate the net force supported by the lithosphere beneath the Ganges basin, given the depth to the neutral fiber. We assume the Moho is 5 km deeper under the Ganges basin than at Bhuj [*Rai et al.*, 2006] and that this 5 km is filled at the surface by sediments which support no appreciable stresses. Because deeper faults can support more differential stress, the crust supports a net compressive force, as shown by the solid line in Figure 6b. Assuming the same friction and mantle flow law as we used above, we find that the lithosphere can support *Copley et al.*'s [2010] estimated net compressive force ( $\sim 5.5 \times 10^{12}$  N/m) if the uppermost mantle is at the brittle failure stress and if the ductile stress for a given depth below the Moho is  $\sim 4$  times higher than farther south. Such an increase in stress corresponds to an increase in strain rate of the same factor (if the deformation is by diffusion creep), which is plausible for the increase in strain rate expected because of the curving of the lithosphere as India underthrusts the Himalaya. Alternatively, this increase in stress may correspond to "geometrical hardening" of India because of its along-strike and across-strike curvature as it underthrusts the Tibetan Plateau, in the same manner as described for subduction zones by *Mahadevan et al.* [2010]. Brittle behavior extending into the uppermost mantle is consistent with the 51 km depth of the 1988 Udaypur earthquake ( $87^\circ\text{E}$ ,  $27^\circ\text{N}$  in Figure 1) [*Chen*

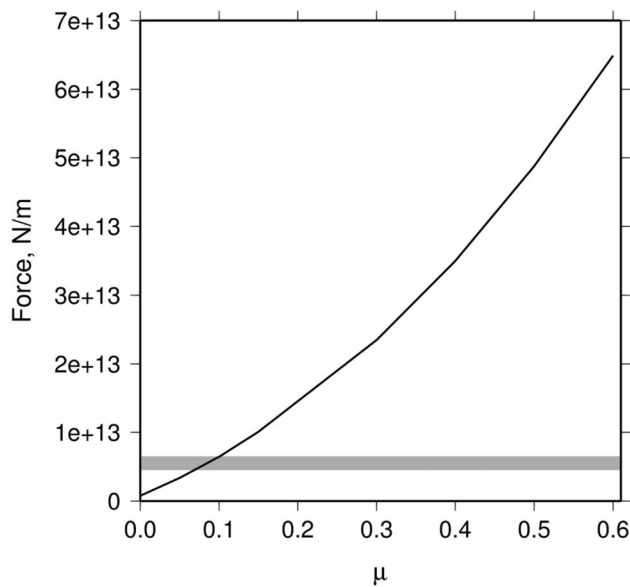


**Figure 7.** The relationship between the coefficient of friction and the force required to be transmitted through the Indian lithosphere in order to replicate the observed depth to the neutral fiber in the Ganges foreland basin (if the lithosphere fails in extension between 5 and 20 km and compression between 29 and 54 km). We have taken the force supported in the ductile layer to be the same as that shown in Figure 6b. The gray shading shows the force that Copley et al. [2010] estimated to be transmitted through the Indian lithosphere.

and Kao, 1996] and the distribution of seismicity south of the Himalaya in eastern Nepal recorded by Monsalve et al. [2006] (Figure 6b).

[26] We have also estimated, for alternative values of the coefficient of friction, the net force that would need to be transmitted through the Indian lithosphere beneath the Ganges foreland basin in order to result in an elastic core at depths of 20–30 km. We find the net force to increase approximately linearly from  $\sim 6.5 \times 10^{12}$  N/m for  $\mu = 0.1$  to  $\sim 6.5 \times 10^{13}$  N/m for a more standard value of  $\mu = 0.6$  (Figure 7). This latter value of  $\mu$  would require a force transmitted through the seismogenic portion of the crust that is roughly an order of magnitude higher than available estimates of the total force transmitted through the lithosphere.

## 5. Conclusions

[27] We have used seismic and geodetic data to study the distribution of slip in the Bhuj earthquake. The event ruptured the crust from the surface to a depth of 25–30 km. The high stress drop ( $\sim 35$  MPa) implies a coefficient of friction of  $\sim 0.08$ , an estimate close to that obtained by assuming that the compressive force resulting from the India-Asia collision is entirely supported by the seismogenic crust. Where India underthrusts southern Tibet, the increase in strain rate associated with the deepening of the Moho leads to seismicity in the very upper mantle, although the majority of the net compressive force is supported by the crust. Our rheo-

logical model, which can explain the seismicity at Bhuj and beneath the Ganges foreland basin, requires the stress level in the crust to be controlled by faults with low friction.

[28] **Acknowledgments.** We thank the Gordon and Betty Moore Foundation for funding this study through the Caltech Tectonics Observatory and Pembroke College in the University of Cambridge for financial support to A.C. We are grateful to D. Schmidt and R. Bürgmann for providing us with their InSAR results. Two anonymous reviewers provided helpful comments on the manuscript.

## References

- Ambraseys, N., and R. Bilham (2003), Reevaluated intensities for the great Assam earthquake of 12 June 1897, Shillong, India, *Bull. Seismol. Soc. Am.*, *93*, 655–673, doi:10.1785/0120020093.
- Antolik, M., and D. S. Dreger (2003), Rupture process of the 26 January 2001  $M_w$  7.6 Bhuj, India, earthquake from teleseismic broadband data, *Bull. Seismol. Soc. Am.*, *93*, 1235–1248, doi:10.1785/0120020142.
- Avouac, J.-P., F. Ayoub, S. Leprince, O. Konca, and D. V. Helmlberger (2006), The 2005,  $M_w$  7.6 Kashmir earthquake: Sub-pixel correlation of ASTER images and seismic waveforms analysis, *Earth Planet. Sci. Lett.*, *249*, 514–528.
- Banerjee, P., R. Bürgmann, B. Nagarajan, and E. Apel (2008), Intraplate deformation of the Indian subcontinent, *Geophys. Res. Lett.*, *35*, L18301, doi:10.1029/2008GL035468.
- Bettinelli, P., J.-P. Avouac, M. Flouzat, F. Jouanne, L. Bollinger, P. Willis, and G. R. Chitrakar (2006), Plate motion of India and interseismic strain in the Nepal Himalaya from GPS and DORIS measurements, *J. Geod.*, *80*, 567–589.
- Bilham, R. (1999), Slip parameters for the Rann of Kachchh, India, 16 June 1819 earthquake, quantified from contemporary accounts, in *Coastal Tectonics*, edited by I. S. Stewart and C. Vita-Finzi, *Geol. Soc. Spec. Publ.*, *146*, 295–318.
- Bilham, R., and P. England (2001), Plateau pop-up during the 1897 Assam earthquake, *Nature*, *410*, 806–809.
- Bodin, P., and S. Horton (2004), Source parameters and tectonic implications of aftershocks of the  $M_w$  7.6 Bhuj earthquake of 26 January 2001, *Bull. Seismol. Soc. Am.*, *94*, 818–827.
- Bollinger, L., J. P. Avouac, R. Cattin, and M. R. Pandey (2004), Stress buildup in the Himalaya, *J. Geophys. Res.*, *109*, B11405, doi:10.1029/2003JB002911.
- Bürgmann, R., D. D. Pollard, and S. J. Martel (1994), Slip distributions on faults: Effects of stress gradients, inelastic deformation, heterogeneous host-rock stiffness, and fault interaction, *J. Struct. Geol.*, *16*, 1675–1690.
- Chandrasekhar, D. V., D. C. Mishra, B. Singh, V. Vijayakumar, and R. Bürgmann (2004), Source parameters of the Bhuj earthquake, India of January 26, 2001 from height and gravity changes, *Geophys. Res. Lett.*, *31*, L19608, doi:10.1029/2004GL020768.
- Chandrasekhar, D. V., R. Bürgmann, C. D. Reddy, P. S. Sunil, and D. A. Schmidt (2009), Weak mantle in NW India probed by geodetic measurements following the 2001 Bhuj earthquake, *Earth Planet. Sci. Lett.*, *280*, 229–235.
- Chen, W.-P., and P. Molnar (1983), Focal depths of intracontinental and intraplate earthquakes and their implications for the thermal and mechanical properties of the lithosphere, *J. Geophys. Res.*, *88*(B5), 4183–4214.
- Chen, W.-P., and H. Kao (1996), Seismotectonics of Asia: Some recent progress, in *The Tectonic Evolution of Asia*, edited by A. Yin and M. Harrison, pp. 37–62, Cambridge Univ. Press, New York.
- Copley, A., J.-P. Avouac, and J.-Y. Royer (2010), India-Asia collision and the Cenozoic slowdown of the Indian plate: Implications for the forces driving plate motions, *J. Geophys. Res.*, *115*, B03410, doi:10.1029/2009JB006634.
- Copley, A., J.-P. Avouac, and B. P. Wernicke (2011), Evidence for mechanical coupling and strong Indian lower crust beneath southern Tibet, *Nature*, *472*, 79–81, doi:10.1038/nature09926.
- Gahalaut, V. K., and R. Bürgmann (2004), Constraints on the source parameters of the 26 January 2001 Bhuj, India, earthquake from satellite images, *Bull. Seismol. Soc. Am.*, *94*, 2407–2413, doi:10.1785/0120040021.
- Gupta, H. K. (2002), A review of recent studies of triggered earthquakes by artificial water reservoirs with special emphasis on earthquakes in Koyna, India, *Earth Sci. Rev.*, *58*, 279–310, doi:10.1016/S0012-8252(02)00063-6.
- Herman, F., et al. (2010), Exhumation, crustal deformation, and thermal structure of the Nepal Himalaya derived from the inversion of thermochronological and thermobarometric data and modeling of the topography, *J. Geophys. Res.*, *115*, B06407, doi:10.1029/2008JB006126.

- Hetényi, G., R. Cattin, J. Vergne, and J. L. Nábělek (2006), The effective elastic thickness of the India Plate from receiver function imaging, gravity anomalies and thermomechanical modelling, *Geophys. J. Int.*, *167*, 1106–1118, doi:10.1111/j.1365-246X.2006.03198.x.
- Hirth, G., and D. Kohlstedt (2003), Rheology of the upper mantle and the mantle wedge: A view from the experimentalists, in *Inside the Subduction Factory*, *Geophys. Monogr. Ser.*, vol. 138, edited by J. Eiler, pp. 83–105, AGU, Washington, D. C.
- Huenges, E., J. Erzinger, J. Kück, B. Engeser, and W. Kessels (1997), The permeable crust: Geohydraulic properties down to 9101 m depth, *J. Geophys. Res.*, *102*(B8), 18,255–18,265, doi:10.1029/96JB03442.
- Jackson, J., D. McKenzie, K. Priestley, and B. Emmerson (2008), New views on the structure and rheology of the lithosphere, *J. Geol. Soc.*, *165*, 453–465, doi:10.1144/0016-76492007-109.
- Ji, C., D. J. Wald, and D. V. Helmberger (2002), Source description of the 1999 Hector Mine, California, earthquake, Part I: Wavelet domain inversion theory and resolution analysis, *Bull. Seismol. Soc. Am.*, *92*, 1192–1207, doi:10.1785/0120000916.
- Ji, C., D. V. Helmberger, D. J. Wald, and K.-F. Ma (2003), Slip history and dynamic implications of the 1999 Chi-Chi, Taiwan, earthquake, *J. Geophys. Res.*, *108*(B9), 2412, doi:10.1029/2002JB001764.
- Johanson, I. A., and R. Bürgmann (2010), Coseismic and postseismic slip from the 2003 San Simeon earthquake and their effects on backthrust slip and the 2004 Parkfield earthquake, *J. Geophys. Res.*, *115*, B07411, doi:10.1029/2009JB006599.
- Jónsson, S., H. Zebker, P. Segall, and F. Amelung (2002), Fault slip distribution of the 1999  $M_w$  7.1 Hector Mine, California, earthquake, estimated from satellite radar and GPS measurements, *Bull. Seismol. Soc. Am.*, *92*, 1377–1389, doi:10.1785/0120000922.
- Konca, A. O., et al. (2008), Partial rupture of a locked patch of the Sumatra megathrust during the 2007 earthquake sequence, *Nature*, *456*, 631–635, doi:10.1038/nature07572.
- Konca, A. O., S. Leprince, J.-P. Avouac, and D. V. Helmberger (2010), Rupture process of the 1999  $M_w$  7.1 Duzce earthquake from joint analysis of SPOT, GPS, InSAR, strong-motion, and teleseismic data: A super-shear rupture with variable rupture velocity, *Bull. Seismol. Soc. Am.*, *100*, 267–288.
- Lamb, S. (2006), Shear stresses on megathrusts: Implications for mountain building behind subduction zones, *J. Geophys. Res.*, *111*, B07401, doi:10.1029/2005JB003916.
- Leprince, S., S. Barbot, F. Ayoub, and J.-P. Avouac (2007), Automatic and precise ortho-rectification, coregistration, and subpixel correlation of satellite images, application to ground deformation measurements, *IEEE Trans. Geosci. Remote Sens.*, *45*, 1529–1558.
- Leprince, S., P. Muse, and J.-P. Avouac (2008), In-flight CCD distortion calibration for pushbroom satellites based on subpixel correlation, *IEEE Trans. Geosci. Remote Sens.*, *46*, 2675–2683.
- Mahadevan, L., R. Bendick, and H. Liang (2010), Why subduction zones are curved, *Tectonics*, *29*, TC6002, doi:10.1029/2010TC002720.
- Mandal, P., R. Narsaiah, B. Sairam, C. Satyamurty, and I. P. Raju (2006), Relocation of early and late aftershocks of the 2001 Bhuj earthquake using joint hypocentral determination (JHD) technique: Implication toward the continued aftershock activity for more than four years, *Pure Appl. Geophys.*, *163*, 1561–1581, doi:10.1007/s00024-006-0090-6.
- McKenzie, D. (1984), The generation and compaction of partially molten rock, *J. Petrol.*, *25*, 713–765, doi:10.1093/petrology/25.3.713.
- Mishra, D. C., D. V. Chandrasekhar, and B. Singh (2005), Tectonics and crustal structures related to Bhuj earthquake of January 26, 2001: Based on gravity and magnetic surveys constrained from seismic and seismological studies, *Tectonophysics*, *396*, 195–207, doi:10.1016/j.tecto.2004.12.007.
- Molnar, P., and H. Lyon-Caen (1988), Some simple physical aspects of the support, structure, and evolution of mountain belts, *Spec. Pap. Geol. Soc. Am.*, *218*, 179–207.
- Monsalve, G., A. Sheehan, V. Schulte-Pelkum, S. Rajaure, M. R. Pandey, and F. Wu (2006), Seismicity and one-dimensional velocity structure of the Himalayan collision zone: Earthquakes in the crust and upper mantle, *J. Geophys. Res.*, *111*, B10301, doi:10.1029/2005JB004062.
- Negishi, H., J. Mori, T. Sato, R. Singh, S. Kumar, and N. Hirata (2002), Size and orientation of the fault plane for the 2001 Gujarat, India earthquake ( $M_w$  7.7) from aftershock observations: A high stress drop event, *Geophys. Res. Lett.*, *29*(20), 1949, doi:10.1029/2002GL015280.
- Priestley, K., J. Jackson, and D. McKenzie (2008), Lithospheric structure and deep earthquakes beneath India, the Himalaya and southern Tibet, *Geophys. J. Int.*, *172*, 345–362, doi:10.1111/j.1365-246X.2007.03636.x.
- Rai, S. S., K. F. Priestley, V. K. Gaur, S. Mitra, M. P. Singh, and M. Searle (2006), Configuration of the Indian Moho beneath the NW Himalaya and Ladakh, *Geophys. Res. Lett.*, *33*, L15308, doi:10.1029/2006GL026076.
- Rao, B. R. (2000), Historical seismicity and deformation rates in the Indian peninsular shield, *J. Seismol.*, *4*, 247–258, doi:10.1023/A:1009863312431.
- Rao, B. R., and P. S. Rao (1984), Historical seismicity of peninsular India, *Bull. Seismol. Soc. Am.*, *74*, 2519–2533.
- Rao, N. P., T. Tsukuda, M. Kosuga, S. C. Bhatia, and G. Suresh (2002), Deep lower crustal earthquakes in central India: Inferences from analysis of regional broadband data of the 1997 May 21, Jabalpur earthquake, *Geophys. J. Int.*, *148*, 132–138, doi:10.1046/j.0956-540x.2001.01584.x.
- Rolandone, F., R. Bürgmann, and R. M. Nadeau (2004), The evolution of the seismic-aseismic transition during the earthquake cycle: Constraints from the time-dependent depth distribution of aftershocks, *Geophys. Res. Lett.*, *31*, L23610, doi:10.1029/2004GL021379.
- Sarkar, D., K. Sain, P. R. Reddy, R. D. Catchings, and W. D. Mooney (2007), Seismic-reflection images of the crust beneath the 2001  $M = 7.7$  Kutch (Bhuj) epicentral region, western India, *Spec. Pap. Geol. Soc. Am.*, *425*, 319–327.
- Schmidt, D. A., and R. Bürgmann (2006), InSAR constraints on the source parameters of the 2001 Bhuj earthquake, *Geophys. Res. Lett.*, *33*, L02315, doi:10.1029/2005GL025109.
- Seeber, L., G. Ekström, S. K. Jain, C. V. R. Murty, N. Chandak, and J. G. Armbruster (1996), The 1993 Killari earthquake in central India: A new fault in Mesozoic basalt flows?, *J. Geophys. Res.*, *101*(B4), 8543–8560.
- Sleep, N. H., and M. L. Blanpied (1992), Creep, compaction and the weak rheology of major faults, *Nature*, *359*, 687–692, doi:10.1038/359687a0.
- Suppe, J. (2007), Absolute fault and crustal strength from wedge tapers, *Geology*, *35*, 1127–1130, doi:10.1130/G24053A.1.
- Talwani, P., and A. Gangopadhyay (2001), Tectonic framework of the Kachchh earthquake of 26 January 2001, *Seismol. Res. Lett.*, *72*, 336–345, doi:10.1785/gssrl.72.3.336.
- Townend, J., and M. D. Zoback (2000), How faulting keeps the crust strong, *Geology*, *28*, 399–402, doi:10.1130/0091-7613(2000)28<399:HFKTC>2.0.CO;2.
- Turcotte, D. L., and G. Schubert (2002), *Geodynamics*, 2nd ed., Cambridge Univ. Press, Cambridge, U. K.
- Wallace, K., R. Bilham, F. Blume, V. K. Gaur, and V. Gahalaut (2006), Geodetic constraints on the Bhuj 2001 earthquake and surface deformation in the Kachchh Rift Basin, *Geophys. Res. Lett.*, *33*, L10301, doi:10.1029/2006GL025775.
- Watts, A. B., and E. B. Burov (2003), Lithospheric strength and its relationship to the elastic and seismogenic layer thickness, *Earth Planet. Sci. Lett.*, *213*, 113–131, doi:10.1016/S0012-82X(03)00289-9.
- Wesnowsky, S. G., L. Seeber, T. K. Rockwell, V. Thakur, R. Briggs, S. Kumar, and D. Ragona (2001), Eight days in Bhuj: Field report bearing on surface rupture and genesis of the 26 January 2001 earthquake in India, *Seismol. Res. Lett.*, *72*, 514–524, doi:10.1785/gssrl.72.5.514.

J.-P. Avouac, J. Hollingsworth, and S. Leprince, Tectonics Observatory, Division of Geological and Planetary Sciences, California Institute of Technology, 1200 E. California Blvd., Pasadena, CA 91125, USA.

A. Copley, COMET+, Bullard Laboratories, Department of Earth Sciences, University of Cambridge, Madingly Rise, Cambridge CB3 0EZ, UK. (acc41@cam.ac.uk)